Superalloys 2004
Edited by K.A. Green, T.M. Pollock, H. Harada,
T.E. Howson, R.C. Reed, J.J. Schirra, and S. Walston
TMS (The Minerals, Metals & Materials Society), 2004

FATIGUE CRACK GROWTH BEHAVIOUR UNDER MIXED MODE LOADING IN UDIMET 720 SX

M.R. Joyce and P.A.S. Reed
Materials Research Group, School of Engineering Science, University of Southampton, Southampton, UK.

Keywords: Nickel Base Single Crystal, Fatigue, High Temperature, Mixed-Mode

Abstract

The effect of temperature and loading mode on the fatigue crack growth behaviour of UDIMET 720 single crystals has been examined. Stage I fatigue crack growth was promoted by mixed mode loading and plane stress conditions. Increasing the temperature to 650 °C has been shown to suppress stage I growth at low ΔK, but to apparently increase slip planarity at higher ΔK levels. By analysing crack paths it has been shown that during planar stage I propagation preferentially activated slip systems may be predicted by considering the resolved stress intensity factors acting along them with respect to the nominal crack plane. Furthermore, during homogeneous stage II propagation crack growth direction may be characterised in terms of the maximum tangential stress. An effective stress intensity factor ΔK_{eq} has been shown to correlate fatigue crack growth rates under pure mode I and mixed mode conditions for the Stage II propagation mechanism, thereby showing that the greatly enhanced crack growth rates observed during stage I propagation c.f. stage II on the basis of ΔK_{eq} are due to this being an intrinsically faster growth mechanism.

Introduction

In highly stressed components, such as turbine discs, much of the fatigue lifetime is taken up by the nucleation and early growth of fatigue cracks. It is widely recognised that such small flaws grow principally in Stage I and at higher rates than larger defects under the same nominal ΔK [1,2]. This behaviour poses problems for component lifing and is generally attributed to a number of factors; (1) crack length is short compared to the crack tip plasticity, hence the LEFM assumption of similitude is invalid; (2) short cracks are unlikely to have sufficient wake for closure levels equivalent to those found in long flaws to develop; (3) short cracks are considerably more sensitive to local microstructure. This final point is a particular problem when attempting to characterise stage I behaviour, since extrinsic factors (grain orientation, grain angle boundary, etc) will also effect fatigue crack growth rate, and may serve to obscure the intrinsic stage I growth.

Use of single crystal specimens can offer a significant advantage since the entire specimen may be regarded as a single grain. Furthermore Ni based superalloys exhibit low stacking fault energies and are susceptible to highly planar slip processes. As a result stage I type growth can be significant in these alloys making them ideal for studying intrinsic stage I behaviour. Whilst the crack growth behaviour of single crystal alloys is of interest to the turbine blade community, the more highly stressed turbine discs are generally polycrystalline. It is important to recognise the possible effect of compositional differences, therefore the material used in this study was single crystal Udimet 720 (a typical disc alloy). Tests were carried out to investigate the effect of temperature under both pure mode I and mixed mode loading conditions.

Experimental

Single edge notch bend (SENB) samples were produced by EDM machining with nominal dimensions 12×12×60 mm. The specimens were removed such that their long axis was in the <001> direction and notched to give a $\langle \bar{1}\,\bar{1}\,0 \rangle$ nominal crack growth direction, as shown in Figure 1.

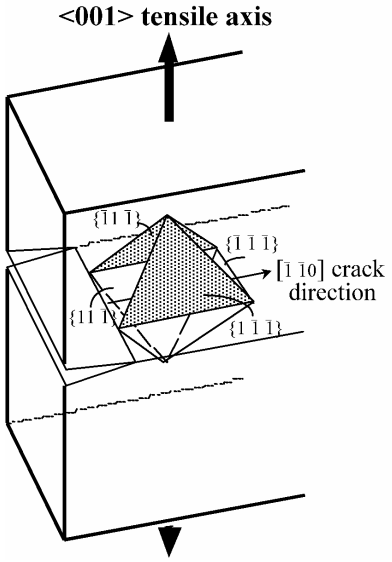

Figure 1: Single crystal sample orientation

The precursor notch was cut 3 mm deep (giving an initial a/W of 0.25) and sharpened with a razor blade before testing. Fatigue tests were carried out using a Instron 8501 servo-hydraulic machine equipped with an ESH environmental chamber using quartz lamps for sample heating. Testing temperatures of 20°C and 650°C were considered, temperature being controlled by a Eurotherm 2416 to ± 1 °C via a Pt/Pt-Rb thermocouple spot welded directly to the sample. All testing was carried out at a load ratio of 0.1 using the four point pulsed direct current potential drop technique for crack monitoring. The use of a pulsed system eliminates false readings produced by electrical closure effects, since the potential drop is measured only at maximum load and hence at maximum crack opening. Pre-cracking was carried out at test temperature in symmetric four-point bend (S4P) at a frequency of 20Hz at a constant ΔK of 25 MPa√m. After crack initiation and steady growth for an indicated length of 1 mm, a

load shedding routine was used to determine fatigue threshold. This entailed reducing the applied ΔK in 10% increments each time the crack extended through four monotonic plastic zone sizes. Threshold was deemed reached when the indicated fatigue crack growth rate had reduced below 1×10^{-7} mm/cycle. The remainder of the test was carried out under constant load range (increasing ΔK) conditions at a load ratio of 0.1 using a 1-1-1-1 waveform. Comprising a 1 second dwell at maximum and minimum loads, with ramp times of 1 second, giving a overall loading frequency of 0.25 Hz. Tests were performed in either pure mode I loading using S4P or in mixed mode loading using an Antisymmetric four point bend geometry (AS4P), these are shown in Figure 2.

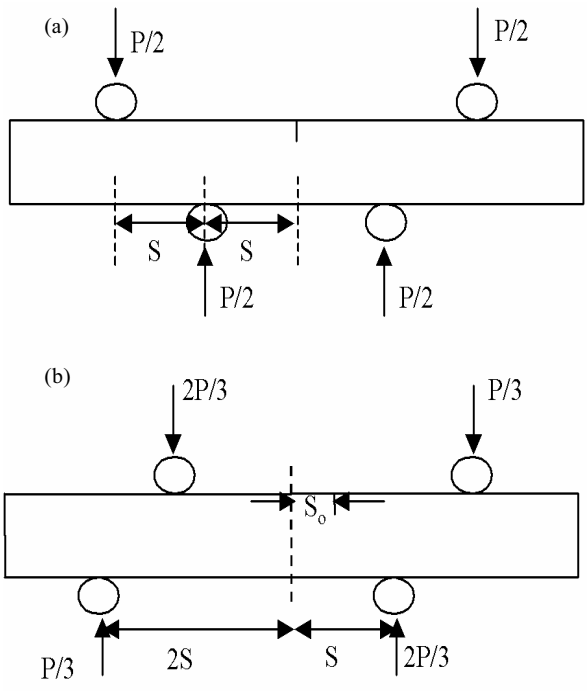

Figure 2: Bend test loading geometries (a) S4P; and (b) AS4P

In the AS4P geometry, the initial mode mixity (K_I/K_{II} ratio) is controlled by the distance between the crack tip and the sample centre line, S_0, which was calculated using Eqn 1.

$$\frac{K_I}{K_{II}} = \frac{S_0}{W}\frac{Y_I}{Y_{II}} \tag{1}$$

with absolute values or K_I and K_{II} being calculated from the known bending moment and shear force values, denoted M and Q respectively in Eqns 2 and 3.

$$K_I = \frac{Y_I M}{BW^{\frac{3}{2}}} \tag{2}$$

$$K_{II} = \frac{Y_{II} Q}{BW^{\frac{1}{2}}} \tag{3}$$

Where Y_I and Y_{II} are appropriate compliance functions for bending and shear. These were determined using a simple finite element analysis based on the work of He et al [3] to calculate the mixed mode stress intensity factors at the crack tip. All the tests presented in this work were carried out with an initial mode mixity of 1.8. However the compliance functions are non-linear and depend on crack length, hence the crack tip mode mixity alters as the crack extends and this change must be accounted for when interpreting the results.

Tests were run until the indicated crack length reached an a/W of 0.75 at which point the samples were broken open to allow examination of the fracture surface. This was performed optically and using a Jeol JSM 6500F field emission gun scanning electron microscope (FEGSEM) operating at 25 kV. Fracture surfaces were also electro-nickel plated using a Watt's Nickel plate solution (150g $NiSO_4$, 20g $NiCl_2$ and 20g H_3BO_3 in 500ml distilled water) operated at 55-60 °C for 15 minutes. The plated fracture surfaces were then sectioned, polished and etched before SEM examination. A Nimonic etch (10ml HNO_3, 50ml HCl, 2.5g $CuCl_2$, 40ml H_2O) was used to etch preferentially the γ' to reveal deformation and failure mechanisms occurring behind the fracture surface.

General Observation and Fractography

Room Temperature Tests

Optical fracture surface overviews of tests performed under pure mode I and mixed mode loading are shown in Figures 3 and 4 respectively. In both cases, macroscopically the crack remained planar with the initial notch. Fatigue crack growth under pure mode I loading is almost exclusively by an apparently stage II type mechanism, however stage I type facets are evident at crack initiation sites and more extensively at the sample sides.

Figure 3: Optical micrograph of fracture surface produced at room temperature under pure mode I loading

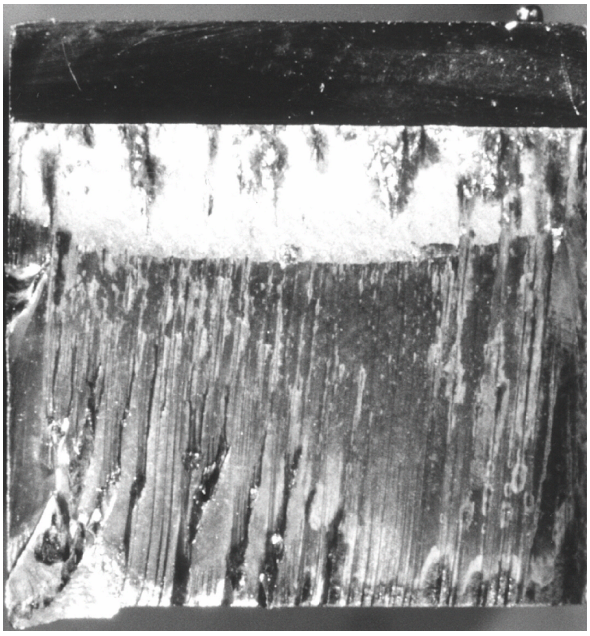

Figure 4: Optical micrograph of fracture surface produced at room temperature under mixed mode loading

Sectioning studies of these latter features shows classical propagation along the $\{\bar{1}\,1\,\bar{1}\}$ and $\{1\,\bar{1}\,\bar{1}\}$ "roof top" planes (shaded planes in Figure 1) with evident shearing of the γ' precipitates. In contrast, mixed mode loading appears to strongly promote a stage I type growth mechanism. Figure 5 shows the abrupt change in growth mechanism from the generally stage II type produced in the pure mode I pre-crack to the stage I type growth produced under mixed mode loading.

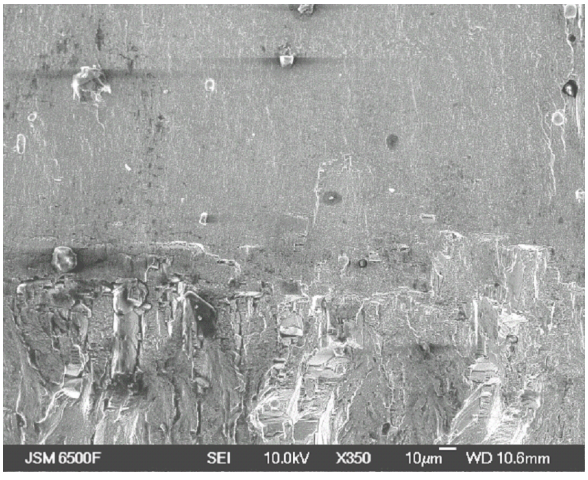

Figure 5: SEM micrograph showing room temperature fracture surface showing transition to mixed mode loading

Figure 6 shows a section normal to the nominal crack growth direction, extensive bands are clearly visible and crack growth occurs along the "roof top" slip planes forming large facets co-linear with the nominal crack growth direction.

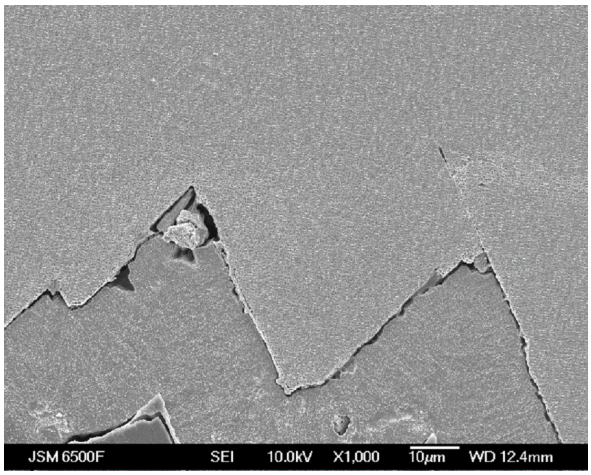

Figure 6: Section through room temperature fracture surface normal to the nominal crack growth direction showing crystallographic facets formed during mixed mode propagation.

Elevated Temperature Fatigue Tests

The fracture surfaces produced in the elevated temperature tests are shown in Figures 7 and 8 respectively. In contrast to the room temperature tests, significant macroscopic deflection was observed in both tests at elevated temperature as shown in Figures 9a and 9b for the pure mode I and mixed mode cases respectively.

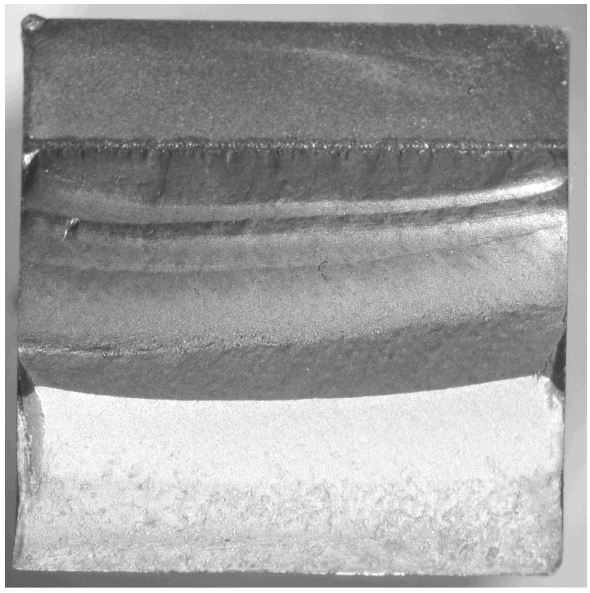

Figure 7: Optical micrograph of fracture surface produced at 650°C under pure mode I loading.

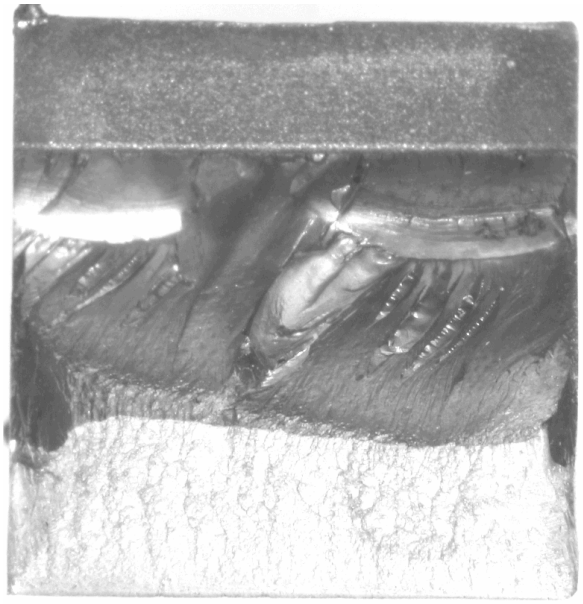

Figure 8: Optical micrograph of fracture surface produced at 650°C under mixed mode loading

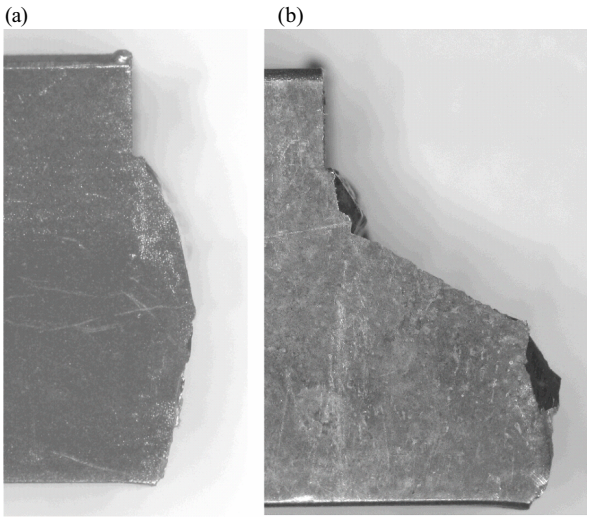

Figure 9: Macroscopic crack deflection Seen in (a) pure mode I test; and (b) mixed mode test.

Significant oxidation of the fracture surface, apparently preferentially attacking the γ', was observed in the pre-crack and during the decreasing ΔK regions. In the test performed under pure mode I loading, facets were evident at crack initiation points and significant early growth occurred along the "factory roof" planes (denoted $\{1\,1\,\bar{1}\}$ and $\{\bar{1}\,\bar{1}\,\bar{1}\}$ in Figure 1) before changing to a stage II type mechanism and deflecting back to the nominal crack growth direction. Generally fatigue crack growth occurred by a stage II type mechanism, however, in contrast to the room temperature tests, a degree of macroscopic crack deflection was observed, principally due to the stage I type early growth. At ΔK levels above ~25 MPavm the crack was observed to revert back to propagation along the "factory roof" planes until failure. Additionally small side facets were observed in this region.

The fracture surface produced under mixed mode loading is more complex. Two separate initiation points are clearly evident in the mode I pre-crack, and significant stage I facets are evident. During the decreasing ΔK portion of the test, the growth mechanism became more stage II like. However the crack remained macroscopically tortuous due to significant deflection in the facetted pre-crack. On the transition to mixed mode loading the growth mechanism remained stage II, however the crack deflected sharply. Facet features appear on the fracture surface in this region both at the sample edges and within the bulk. Whilst the side facets are clearly crystallographic, the central features do not correspond with crystallographic planes rather they appear aligned along the dendrites. Sectioning studies show crack propagation along clearly defined crystallographic planes at the sample sides. However, whilst the central features are clearly defined, the crack propagation remains apparently stage II like, as shown in Figure 10.

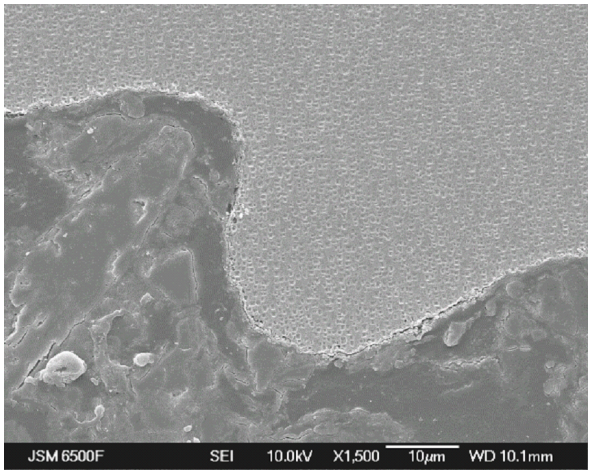

Figure 10: SEM micrograph of a section through the elevated temperature fracture surface normal to the nominal crack growth direction showing un-crystallographic facet like features during propagation under mixed mode loading

It is interesting to note that in both tests at elevated temperature significantly more crystallographic crack propagation was seen during pre-cracking than in the room temperature tests. In both cases this led to macroscopic crack deflection, which was not corrected until a stage II type crack propagation mechanism was established.

Fatigue Crack Growth Analysis

To allow analysis and comparison of test results, accurate assessment of the crack tip stress state is required. Calculation of K_I and K_{II} in the room temperature pure mode 1 test was reasonably simple, since macroscopic crack growth occurred in the nominal direction and therefore the analytical expression given in Eqn 1 is valid. Whilst the crack produced under mixed mode loading at room temperature is macroscopically planar, it is significantly faceted. Therefore a simple finite element study was

performed to assess the effect of this faceting on the local K levels.

Figure 11 shows how a simple nominally plane strain section was used to approximate the faceted fracture surface. Since the facet angle is fixed (i.e. the 109° angle between $\{\bar{1}\,1\,\bar{1}\}$ and $\{1\,\bar{1}\,\bar{1}\}$ "roof top" planes), the width of the section relative to the width of the overall sample can also be defined in terms of the number of facets in the overall sample. Therefore since the fracture surface produced under mixed loading at room temperature comprised ~40 facets; only 2.5% of the overall specimen width was modelled.

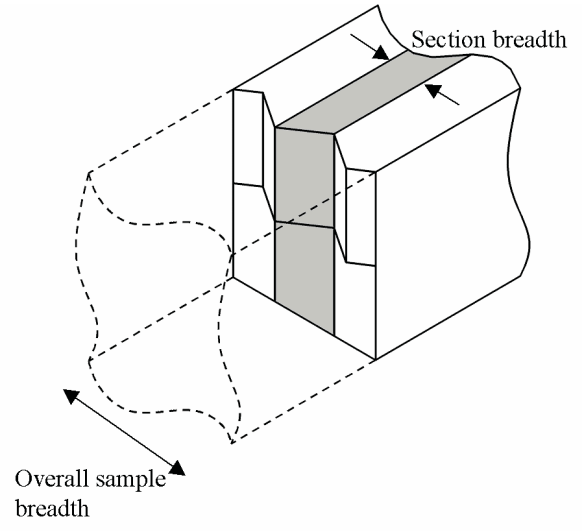

Figure 11: Only the section containing a single facet plane forms FE model.

The finite element model was created using ~6000 20 noded brick elements refined around the crack front. Nodal constraints were applied to represent the lower rollers in the AS4P loading geometry, whilst the magnitude of loading applied to the upper rollers was dependent on the ratio of section to overall sample breadth. Plane strain boundary conditions were applied to the sectioned faces, thereby approximating the stress state in the majority of the full sample width. A linear elastic isotropic material response was assumed and the model solved using the ANSYS6.1 finite element code in a single increment from zero to maximum load. Elastic anisotropy has been ignored, previous work by Chan and Cruse [4] in single crystal samples has indicated that the degree of elastic anisotropy was insufficient to affect K solutions, thereby justifying the isotropic assumption. The model was solved at several increments of crack length and local K values calculated directly from the nodal displacements according to Eqn 4.

$$K_I = \lim_{r \to 0} \left| \sqrt{2\pi} \frac{G}{1+\kappa} \frac{|\Delta v|}{\sqrt{r}} \right|$$

$$K_{II} = \lim_{r \to 0} \left| \sqrt{2\pi} \frac{G}{1+\kappa} \frac{|\Delta u|}{\sqrt{r}} \right|$$

$$K_{III} = \lim_{r \to 0} \left| \sqrt{2\pi} \frac{G}{1+\kappa} \frac{|\Delta w|}{\sqrt{r}} \right| \quad (4)$$

Where Δv, Δu and Δw are the motions of one crack face with respect to the other. To allow comparison with the analytical result for the pure mode I case the calculated K values were expressed as an equivalent stress intensity factor K_{eq} (calculated on the basis of a simple co-planar strain energy release rate criterion given in Eqn 5) and then this factor averaged along the crack front.

$$\Delta K_{eq} = \sqrt{\Delta K_I^2 + \Delta K_{II}^2 + \Delta K_{III}^2} \quad (5)$$

The reduction in crack tip stress intensity factor was found to be reasonably insensitive to crack length over the range considered. Generally K_{eq} was reduced by ~7% by accounting for the "roof top" facets and this was accounted for when comparing crack growth rates.

In contrast to the room temperature tests, the distorted fractures surfaces produced at elevated temperature required the use of full three-dimensional finite element modelling. The fracture surfaces were assessed by an optical profilometer and then approximated using a 10 by 10 grid of points. A finite element model was constructed from these points, comprising ~6500 20 node brick elements, the meshed approximation of the mixed mode test is shown in Figure 12.

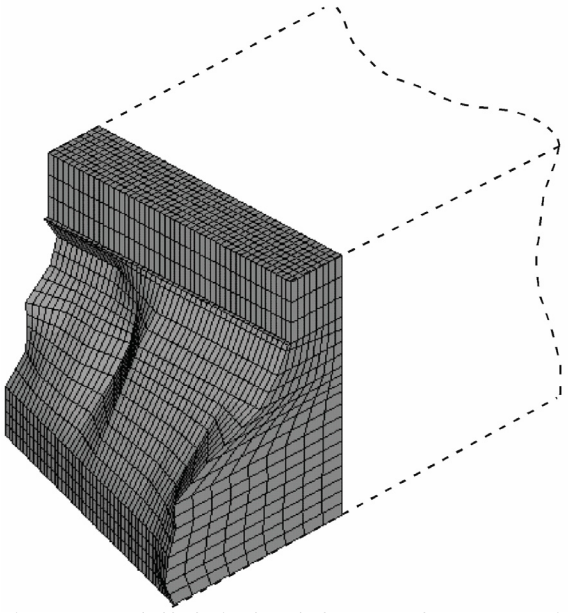

Figure 12: One half of mixed mode fracture surface representation used for three-dimensional finite element model

In all cases the crack front was assumed to be straight through thickness, rather than half penny shaped. Whilst this assumption is clearly invalid within the pre-crack region, it is reasonable within the growth out section of the test to which this analysis is restricted. As previously an isotropic linear elastic material model was applied and the model solved in a single loading step from zero to maximum load. The model was solved repeatedly at several crack length increments. During post

processing local K values were calculated along the crack front directly from the computed nodal displacements according to Eqn 4. As previously the local K values were expressed as K_{eq} and then averaged along the crack front. To allow comparison with the room temperature results in Figure 13.

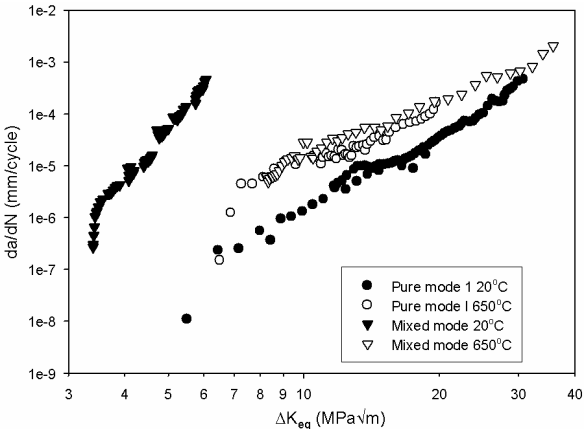

Figure 13: Crack growth rates for all tests correlated using ΔK_{eq}

As expected, under pure mode I loading the fatigue crack growth rate is generally more rapid at 650°C than at room temperature, although the results do seem more comparable near threshold. Despite the highly deflected crack path, the fatigue crack growth rates produced under mixed mode loading at elevated temperature are comparable with those observed under pure mode I loading. In contrast the fatigue crack propagation rates recorded under mixed mode conditions at room temperature are considerably more rapid.

Discussion

Effect of temperature

Considering first the results obtained from the pure mode I loading tests, increasing the test temperature was found to generally increase crack growth rates. This is likely to be linked to a combination of reduced mechanical properties and enhanced oxidation. Typically the crack tip oxidation associated with high temperatures is thought to reduce slip reversibility, in addition increased thermally activated cross slip will also tend to homogenise slip all of which makes stage II behaviour more favourable. It is therefore intriguing that significantly more stage I type crack growth was seen in the pure mode I pre-cracks of both high temperature tests. In the entirely pure mode I test the pre-crack was planar through the sample breadth, however in the mixed mode test two distinct pre-cracks formed on opposite "factory roof" planes, denoted $\{1\,1\,\bar{1}\}$ and $\{\bar{1}\,\bar{1}\,\bar{1}\}$ in Figure 1, causing a complex crack shape to develop. Samples were aligned carefully before testing and as the S4P loading geometry is reasonably insensitive to small crack position misalignments the increased crystallographic behaviour may be linked to the slip character at elevated temperature. It appears that the reduction in mechanical properties at 650°C has overcome the increased slip homogeneity and favoured extended slip band cracking at ΔK levels that produced stable stage II type propagation at room temperature. Whilst the crack is clearly propagating along a slip plane, it does not appear to alternate between pairs of planes to maintain a nominal $\langle \bar{1}\,\bar{1}\,0 \rangle$ crack growth direction, the crack continued to propagate along the plane it initiated in causing significant macroscopic crack deflection. In both elevated temperature tests crack propagation reverted to the nominal direction during the load shedding portion of the test, when a stage II like propagation mechanism appears to become more favourable as the slip bands ahead of the crack tip reduce in length.

Effect of mixed mode loading at 650°C

Despite the highly deflected crack path, the fatigue crack growth rates recorded during propagation under mixed mode loading at 650°C appear comparable with those under pure mode I loading when correlated using either ΔK_I or ΔK_{eq}. Sectioning studies show that in both cases the majority of crack propagation is by a stage II type mechanism, with crystallographic stage I type facets at the sample sides. This demonstrates that planar slip processes are enhanced by a state of plane stress overcoming the more homogeneous cooperative slip operating within the sample bulk.

The marked crack deflection at the onset of mixed mode loading is likely to be linked to the crack deviating such that it experiences the maximum mode I opening. Chan and Leverant [5] tested MAR-M200 single crystals under varying stress states at 982 °C. They found that at this temperature crack propagation occurred in a direction with zero K_{II} component. Erdogan and Sih [6] proposed that crack extension is linked to the resolved tangential stress component. Hence the angle of propagation may be calculated by calculating the radial direction in which the resolved tangential stress is a maximum, and by inference the resolved shear stress zero, according to Eqn 6.

$$\begin{Bmatrix}\sigma_{\theta\theta}\\ \sigma_{r\theta}\end{Bmatrix} = \frac{K_I}{\sqrt{2\pi r}}\cos\left(\frac{\theta}{2}\right)\begin{Bmatrix}\cos^2\left(\frac{\theta}{2}\right)\\ \sin\theta\end{Bmatrix} + \frac{K_{II}}{\sqrt{2\pi r}}\cos\left(\frac{\theta}{2}\right)\begin{Bmatrix}-\frac{3}{2}\sin\theta\\ 3\cos\theta - 1\end{Bmatrix} \quad (6)$$

Where the angle of propagation, θ_0, may be found for any values of K_I and K_{II} by setting the derivative of $\sigma_{\theta\theta}$ with respect to θ equal to zero, and then solving for the case θ equal to θ_0, thereby giving Eqn. 7.

$$K_I \sin\theta_0 + K_{II}(3\cos\theta_0 - 1) = 0 \quad (7)$$

This is clearly equivalent to setting $\sigma_{r\theta}$ equal to zero in Eqn 6, thus giving the requirement that shear stress in the crack growth direction be equal to zero. Local K_I and K_{II} values along the crack front are available from the FE model used previously to obtain ΔK values for crack growth rate correlation, and it is therefore possible to compare the actual crack deflection angle, θ_{act}, with the predicted θ_0 by Eqn 7. Figure 14 shows a contour plot of the discrepancy between these two parameters, it can be seen that Eqn 7 predicts the crack growth direction reasonably well within the specimen bulk. The prediction apparently breaks down at the sample sides, at high crack lengths and in one region at the start of the mixed mode loading. The poor prediction at the sample side and near failure is unsurprising since the propagation in these regions is by a highly crystallographic mechanism rather than by stage II co-operative slip. Furthermore, correlating the region of

poor prediction near the sample centre with the fracture surface overview, it can be seen that this occurs at a point between the two pre-cracks. The local stress state in this region is highly complex and since the pre-cracks are converging, is likely to be of greater influence than that of the nominal crack geometry. This will potentially activate additional crystallographic propagation modes, and hence make the parameter θ_0 insufficient to predict the fatigue crack path.

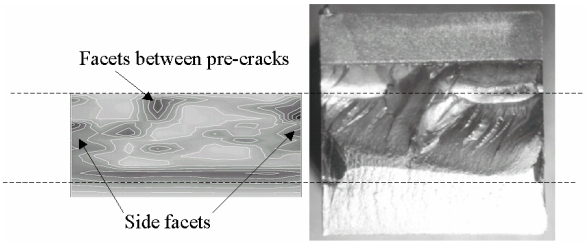

Figure 14: Contour plot of crack path prediction accuracy within mixed mode region. Poor prediction indicated by darker shading, showing correlation with regions of crystallographic growth.

Effect of mixed mode loading at room temperature

As at elevated temperature, the onset of mixed mode loading dramatically affected fatigue crack growth behaviour in the room temperature test. Fatigue crack growth switches to a highly crystallographic stage I dominated mechanism at the onset of mixed mode loading. Furthermore crack growth rates were significantly accelerated compared to those under pure mode I loading whether correlated in terms of ΔK_I or ΔK_{eq}. Seemingly different slip systems are activated by the change in loading mode therefore making a stage I mechanism more favourable than the previous stage II fine scale co-operative slip. Crack deflection as in the elevated temperature test was not observed, rather the crack continued to propagate nominally in the $\langle \bar{1}\,\bar{1}\,0 \rangle$ direction. Continued nominal propagation along $\langle \bar{1}\,\bar{1}\,0 \rangle$ under mixed mode loading will not experience increased mode I opening at the crack tip as crack length increases unlike the elevated temperature crack growth behaviour where the crack deviated to experience the maximum opening stress.

In addition to faster growth, fatigue threshold was considerably reduced, thereby potentially indicating lower closure levels. The alternating $\{\bar{1}\,1\,\bar{1}\}$ and $\{1\,\bar{1}\,\bar{1}\}$ "roof top" planes down which the crack has grown are parallel to the crack growth direction, and previous work [7,8] has suggested that negligible closure will be produced by such a facet morphology under mode I and II opening. A degree of mode III shear is required to bring the facet features into contact before a classic roughness induced closure mechanism can operate. However, such mode III shear is precluded by the plane strain conditions within the sample bulk. Therefore it is likely that roughness induced closure levels will be insignificant through the majority of the sample during stage I propagation along the "roof top" planes, hence contributing to enhanced fatigue crack growth rates during this mode of propagation.

Slip System Analysis

Certain combinations of loading and test environment apparently promote stage I type cracking for any given single crystal orientation. Although only one crystal orientation was considered in the current work, various slip systems were activated during periods of crystallographic growth.

- Significant crack deflection was caused by propagation along "factory roof" planes (e.g. the un-shaded plane marked $\{1\,1\,\bar{1}\}$ in figure 1) during pre-cracking at elevated temperature.
- Side facets along "roof top" planes (e.g. the shaded plane marked $\{1\,\bar{1}\,\bar{1}\}$ in figure 1) were seen in all tests, although more prominently at room temperature.
- Mixed mode loading precipitated faceting along "roof top" planes throughout the sample at room temperature.

In order to elucidate why slip band cracking occurs along certain planes, the interaction between the crack tip stress state and the orientation of the crystal structure with respect to the crack plane must be considered. Telesmann and Ghosn [9] proposed that slip planes preferential for stage I propagation can be identified by their resolved shear stress. Reed *et al* [10] calculated resolved and normal shear stress intensity factors along slip planes and slip directions for both nominal pure mode I and mixed mode stress intensity factors. The analysis of Chen and Liu [11] was used to show that the resolved shear intensity factor, K_{rss}, could be expressed as Eqn 8.

$$K_{rss} = \lim_{r \to 0} \tau_{rss} \sqrt{2\pi r} \tag{8}$$

where r is the distance from the crack tip and τ_{rss} is the resolved shear stress acting on a given slip system at the angle between the slip plane and the crack plane. Eqn 9 proposed by Peach and Koehler [12] gives the value of τ_{rss}.

$$\tau_{rss} = \left(\frac{1}{b}\right) \underline{b} \cdot \underline{\sigma} \cdot \underline{n} \tag{9}$$

where $\underline{b}$ is the slip direction, $\underline{n}$ is the slip plane normal vector, and $\underline{\sigma}$ is the elastic stress tensor. Furthermore the resolved normal stress intensity factor, K_{rns}, can be calculated from an analogous expression. In their analysis Reed et al determine both the K_{rss} and K_{rns} for each slip system at the angle it would make with a nominal pre-crack. Nominal far field loading was applied such that K_I = 4MPa√m in the pure mode I case and K_{eq} = 4MPa√m (K_I = 3.5 MPa√m and K_{II} = 1.94 MPa√m) in the mixed mode case. The results are collated in Table 1, in each slip plane only the highest K_{rss} (and corresponding K_{rns}) of the three possible slip directions is listed. Values are also given for $K_{r(eq)}$, the equivalent resolved stress intensity factor and a K_{rss}/K_{rns} ratio.

Table 1: Resolved stress intensity factors. Favoured slip systems shaded

K_I/K_{II} ratio	Slip planes	Stress state	K_{rss}	K_{rns}	$K_{r(eq)}$	K_{rss}/K_{rns}
PMI	$\{1\bar{1}\,\bar{1}\}$ $\{\bar{1}\,1\,\bar{1}\}$	P. Strain	0.555	3.093	3.142	0.179
PMI	$\{1\,1\,\bar{1}\}$ $\{\bar{1}\,\bar{1}\,\bar{1}\}$	P. Strain	1.255	2.801	3.069	0.448
PMI	$\{1\,\bar{1}\,\bar{1}\}$ $\{\bar{1}\,1\,\bar{1}\}$	P. Stress	1.633	1.333	2.108	1.225
PMI	$\{1\,1\,\bar{1}\}$ $\{\bar{1}\,\bar{1}\,\bar{1}\}$	P. Stress	1.255	2.801	3.069	0.448
1.8	$\{1\,\bar{1}\,\bar{1}\}$ $\{\bar{1}\,1\,\bar{1}\}$	P. Strain	1.111	2.706	2.926	0.411
1.8	$\{1\,1\,1\}$	P. Strain	0.557	4.545	4.578	0.122
1.8	$\{1\,1\,\bar{1}\}$	P. Strain	1.640	0.357	1.678	4.593

Pure mode I tests

Crystallographic stage I propagation along the "factory roof" $\{1\,1\,\bar{1}\}$ planes was seen within the plane strain sample bulk at high ΔK levels and within the pre-crack at elevated temperature. Comparing the resolved stress intensity factors for the $\{1\,1\,\bar{1}\}$ and $\{1\,\bar{1}\,\bar{1}\}$ slip planes under pure mode I loading and plane strain conditions, it can be seen that whilst the $K_{r(eq)}$ values are reasonably similar, the K_{rss}/K_{rns} ratio is significantly higher for the $\{1\,1\,\bar{1}\}$ plane. In contrast the side facets grown under nominally plane stress conditions favoured the $\{1\,\bar{1}\,\bar{1}\}$ "roof top" planes. Under these conditions the $K_{r(eq)}$ value is somewhat larger for the un-favoured slip plane (3.069 c.f. 2.108). However the K_{rss}/K_{rns} ratio is considerably higher for the favoured slip system. Reed et al considered a wider range of orientations and favoured slip systems for Stage I crack growth and proposed a two-parameter criterion for determining slip system selection. Firstly that the K_{rss}/K_{rns} ratio be greater than 0.45 and secondly that $K_{r(eq)}$ be greater than 1.68 (for the same applied far field K values)

Mixed mode tests

At room temperature mixed mode loading produced highly crystallographic growth along the $\{1\,\bar{1}\,\bar{1}\}$ "roof top" planes. With reference to Table 1 it can be seen that unlike the pure mode case the $\{1\,1\,1\}$ and $\{1\,1\,\bar{1}\}$ "factory roof" planes are not equivalent due to the AS4P loading geometry. Furthermore the $\{1\,1\,\bar{1}\}$ plane appears to meet the criteria for preferential selection. However the K_{rns} component of this slip system is very low, therefore little opening displacement will occur across this plane. It is reasonable to assume that both shear and opening modes are required for propagation as originally suggested by Gell and Leverant [13], hence the use of $K_{r(eq)}$ as a criterion for propagation. However $K_{r(eq)}$ alone is insufficient since slip systems which do not exhibit stage I growth may have a high $K_{r(eq)}$ value due to a high K_{rss}, whilst simultaneously having a low K_{rns} value. In contrast to the $\{1\,1\,\bar{1}\}$ plane, the symmetric "roof top" system of the $\{1\,\bar{1}\,\bar{1}\}$ and $\{\bar{1}\,1\,\bar{1}\}$ planes, along which stage I growth was observed to occur, have reasonable amounts of both shearing and opening modes.

Effect of temperature

It is interesting to note that elevated temperature promoted enhanced plane strain stage I crack growth in the pure mode one case whilst crystallographic propagation was suppressed under mixed mode loading. It is thought that this is due to a reduction in mechanical properties at high temperature making extended slip band cracking more favourable during the reasonably high ΔK levels employed during pre-cracking. In contrast the mixed mode test was performed at low ΔK_{eq} levels at which additional thermal activation of cross slip (wavy slip) will favour more homogeneous stage II type behaviour, thereby suppressing the planar Stage I growth seen at room temperature

Conclusions

- Stage I crack growth along certain slip systems is promoted in Udimet 720 single crystals by combinations of plane stress conditions and mixed mode loading Considering the resolved stress intensity factors due to their orientation with respect to the nominal crack growth plane can identify favourable slip systems.

- Increasing the test temperature to 650°C was found to increase extended slip band cracking at high ΔK levels, however increased slip homogeneity was found to entirely suppress stage I growth at low ΔK levels, irrespective of far field loading mode.

- At 650°C, where Stage II crack growth modes predominated, similar crack growth rates were observed under both mixed mode and pure mode I loading when correlated using ΔK_I or ΔK_{eq}. The angle of crack deflection observed under mixed mode loading could be predicted by considering the direction of maximum opening mode during stage II propagation.

- The Stage I crack growth promoted by mixed mode loading at room temperature was considerably faster than the stage II growth observed under pure mode I loading irrespective of correlation factor. Since it has been shown that ΔK_{eq} can account for loading mode at 650°C, where almost all crack growth occurs by stage II, the rapid propagation under mixed mode loading at room temperature must be due to the dominant stage I growth mechanism being intrinsically more rapid.

Acknowledgements

Thanks are due to QinetiQ (formerly DRA Pyestock) for original specimen provision and machining. The support respectively of EPSRC Grant Nos: GR/E93800 and GR/J34309 (PASR) and the British Council/NRC (MRJ) has enabled this collaborative work (CRP project No: 00CRP06) to proceed and is gratefully acknowledged.

References

1. A. Boyd-Lee and J.E. King, "Short fatigue crack path determinants in polycrystalline Ni-base superalloys," *Fat. Fract. Engng. Mater. Struct.*, 17 (1994), 1-14.

2. J. Luo and P. Bowen, "Small and long fatigue crack growth behavior of a PM Ni-based superalloy Udimet 720," *Int. J. Fat.*, 26 (2004), 113-124.

3. M.Y. He, H.C. Cao and A.G. Evans," Mixed mode fracture: The four point shear specimen," *Acta Metall. et Mater.*, 38 (1990), 839-46.

4. K.S. Chan and T.A. Cruse," Stress intensity factors for anisotropic compact-tension specimens with inclined cracks," *Engng. Fract. Mech.,* 23 (1986), 863-74.

5. K.S. Chan and G.R Leverant, "Fatigue crack growth in Mar-M200 single crystals," *Metall. Trans A*, 18A (1987), 593-603.

6. F. Erdogan and G.C. Sih, "On crack extension in plates under plane loading and transverse shear," *Trans. ASME J. Basic Engng*, 85 (1963), 519-27.

7. P.A.S. Reed and J.E. King, "Orientation effects on fatigue crack growth in Udimet 720 single crystals". *Proceeding of the Fifth International Conference on Fatigue and Fatigue Thresholds, Fatigue 93*, eds. J-.P. Bailon and J.L. Dickson (EMAS, Warley, UK 1993), 841-846.

8. K.S. Chan, J.E. Hack and G.R. Leverant, "Fatigue crack propagation in Ni-base superalloy single crystals under multi-axial cyclic loads," *Metall. Trans A*, 17A (1986), 1739-50.

9. J. Telesmann and L.J. Ghosn, "The unusual near threshold fatigue crack growth behavior of a single crystal superalloy and the resolved shear stress as the crack driving force," *Engng Fract. Mech* 34 (1989), 1183-1196.

10. P.A.S. Reed, X.D. Wu and I. Sinclair, "Fatigue crack path predication in Udimet 720 nickel based alloy single crystals," *Metall. et Mater. Trans A*, 31A (2000), 109-123

11. Q. Chen and H.W. Liu: "Resolved Shear Stress Intensity Coefficient and Fatigue Crack Growth in Large Single Crystals" (Contractor Report 182137, NASA, 1988).

12. M.D. Peach and J.S. Koehler, "The forces exerted on dislocations and the stress fields produced by them," *Phys. Review,* 80 (1950), 436-39.

13. M. Gell and G.R. Leverant, "The characteristics of stage I fatigue fractures in a high strength nickel alloy," *Acta Metall.* 16 (1968), 553-61.